Electronic Supporting Information

Enhanced near-infrared phosphorescence found in a structurally similar host–guest system

Tsutomu Ishi-i,[*a] Misuzu Nakaya,[a] Tomoya Umeki,[a] Taisuke Matsumoto,[b] Jun Hyeon Lee,[c] and Takuma Yasuda[c,d]

Table of Contents

Experimental Section

General. All melting points are uncorrected. ATR-IR spectra were recorded on a JASCO FT/IR-470 plus Fourier transform infrared spectrometer, equipped with ATR PRO attachment (Zn-Se prism). ^{1}H and ^{13}C NMR spectra were determined in $CDCl_3$ with a JEOL ECX 500 spectrometer. Residual solvent protons were used as internal standard and chemical shifts (δ) are given relative to tetramethylsilane (TMS). The coupling constants (J) are reported in hertz (Hz). Elemental analysis was performed at the Elemental Analytical Center, Kyushu University. Fast atom bombardment mass spectrometry (FAB-MS) spectra were recorded with a JEOL JMS-70 mass spectrometer with m-nitrobenzyl alcohol (NBA) as a matrix. Gel permeation chromatography (GPC) was performed with a Japan Analytical Industry LC-908 using JAIGEL-1H column (20 × 600 mm) and JAIGEL-2H column (20 × 600 mm) eluting with chloroform (3.0 mL min^{-1}). Analytical TLC was carried out on silica gel coated on aluminum foil (Merck 60 F254). Column chromatography was carried out on silica gel (WAKO C300). Dry THF was purchased from FUJIFILM Wako Pure Chemical Corporation. Dichloromethane and acetic acid were dried over 4A molecular sieves and 3A molecular sieves, respectively, over night before use. 1,2-Dimethoxy-4,5-dinitrobenzene (**1**) and 4,7-dibromo-5,6-dimethoxy-2,1,3-benzothiadiazole (BTD(OMe)-Br) were prepared according to the methods reported previously.[1]

1. T. Ishi-i, R. Kichise, I. S. Park, T. Yasuda and T. Matsumoto, *J. Mater. Chem. C*, 2023, **11**, 3003–3009.

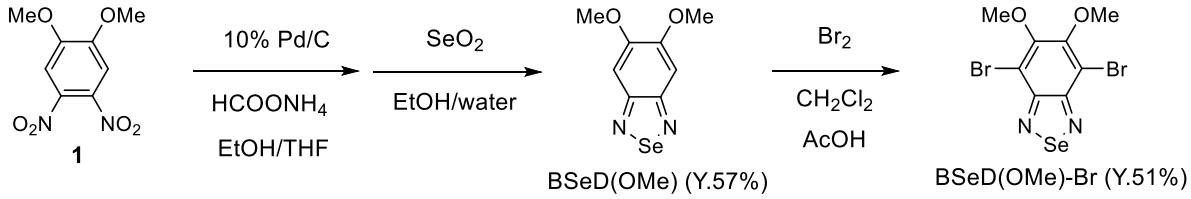

5,6-Dimethoxy-2,1,3-benzoselenodiazole (BSeD(OMe)). To a suspension of **1**[1] (1.73 g, 7.58 mmol) and 10% Pd/C (350 mg) in dry THF (23 mL) and deaerated ethanol (76 mL) was added portionwise ammonium formate (9.58 g, 152 mmol) and the mixture was stirred at room temperature for 1.5 h under an argon atmosphere. The reaction mixture was filtered over celite and wash with deaerated ethanol. The filtrate was evaporated in vacuo to dryness. Without further purification, the crude diamine derivative (3.50 g) was used to the next reaction.

To a mixture of the diamine derivative (3.50 g) in deaerated ethanol (228 mL) was added dropwise selenium dioxide (844 mg, 7.6 mmol) in deaerated distilled water (30 mL) and the mixture was heated at 85 °C for 19 h under an argon atmosphere. The reaction mixture was quenched by addition of water and extracted with chloroform. The combined organic layer was washed with brine and water, dried over anhydrous magnesium sulfate, and evaporated in vacuo to dryness. The residue (1.34 g) was purified by silica gel column chromatography (WAKO C300) eluting with chloroform to give BSeD(OMe) in 57% (1.06 g, 4.34 mmol). An analytical sample was obtained by GPC eluting with chloroform and by recrystallization from hexane/dichloromethane as colorless needles: mp 152–153 °C; IR (ATR, cm^{-1}) 3066, 3036, 2994, 2973, 2935, 2834, 1617, 1538, 1479, 1432, 1327, 1300, 1218, 1168, 1008, 741, 730, 705; ^{1}H NMR ($CDCl_3$, 500 MHz) δ 4.00 (s, 6 H, OMe), 7.01 (s, 2 H, ArH); ^{13}C NMR ($CDCl_3$, 126 MHz) δ 56.34, 99.05, 154.74, 157.25; FAB-MS (positive, NBA) m/z 245 [$(M+1)^+$]. Anal. Calcd for $C_8H_8N_2O_2Se$ (243.12): C, 39.52; H, 3.32; N, 11.52. Found: C, 39.56; H 3.24; N, 11.51.

4,7-Dibromo-5,6-dimethoxy-2,1,3-benzoselenodiazole (BSeD(OMe)-Br). To a solution of BSeD(OMe) (1.34 g, 5.5 mmol) in dry dichloromethane (133 mL) and dry acetic acid (66 mL) was added bromine (5.27 g, 33 mmol) in dry dichloromethane (5 mL) under an argon atmosphere and the mixture was stirred at room temperature for 24 h under dark conditions. After the reaction mixture was quenched by addition of cold water and 1 M aqueous solution of sodium hydrogen sulfite, it was extracted with chloroform. The combined organic layer was washed with 1 M aqueous solution of sodium hydrogen sulfite and water, dried over anhydrous magnesium sulfate, and evaporated in vacuo to dryness. The residue was purified by silica gel column chromatography (WAKO C300) eluting with hexane/chloroform (2:1, v/v) to give BSeD(OMe)-Br in 51% yield (1.13 g, 2.82 mmol). An analytical sample was obtained by GPC eluting with chloroform and by recrystallization from hexane/chloroform as pale yellow needles: mp 214–215 °C; IR (ATR, cm^{-1}) 2943, 2848, 1589, 1480, 1442, 1392, 1276, 1206, 1150, 1035, 968, 940, 819, 755, 736, 646; ^{1}H NMR ($CDCl_3$, 500 MHz) δ4.05 (s, 6 H, OMe); ^{13}C NMR ($CDCl_3$, 126 MHz) δ61.51, 107.77, 154.79, 154.84; FAB-MS (positive, NBA)

m/z 399, 401, 403 [$(M+1)^+$]. Anal. Calcd for $C_8H_6Br_2N_2O_2Se$ (400.91): C, 23.97; H, 1.51; N, 6.99. Found: C, 23.83; H 1.46; N, 6.83.

Instrumentation. Steady-state photoluminescence spectra and excitation spectra were measured on a JASCO FP-8600 fluorescence spectrophotometer. Absorption spectra were measured on a JASCO V-570 spectrophotometer. Diffuse reflection spectra were measured on a JASCO V-670 spectrophotometer equipped with a JASCO ISV-922 integrating sphere system. The fluorescence and phosphorescence quantum yields were measured with an absolute photoluminescence quantum yield measurement system (Hamamatsu Photonics, Quantaurus-QY C11347-01 and C9920-01). This instrument consisted of an integrating sphere equipped with a monochromatized Xe arc lamp as the light source and a multichannel spectrometer. The sensitivity of this system was fully calibrated using deuterium and halogen standard light sources. Fluorescence lifetime measurements were made by using a laser diode (340 nm, pulse width 100 ps, repetition rate 20 kHz) and as the excitation light source and a time-correlated single-photon counting fluorometer (Hamamatsu Photonics, Quantaurus-Tau C11367). For phosphorescence lifetime measurements, a LED diode (340 nm, pulse width 1 ns, repetition rate 2 kHz) was used as the excitation light source. The analysis of the fluorescence and phosphorescence decay curves were carried out using the deconvolution method. Differential scanning calorimetry was performed on a METTLER TOLEDO DSC822e at heating and cooling rates of 10 K min^{-1} under a nitrogen atmosphere. Thermogravimetric analysis (TGA) was performed on a Shimadzu GTD-6AH at heating rate of 10 K min^{-1} under a nitrogen atmosphere. Powder X-ray diffraction measurements were performed on RIGAKU RINT-TTR III and carried out with Cu(Kα) radiation from an X-ray tube with a 0.5 × 10 mm^2 filament operated at 50 kV × 300 mA (15 kW).

Preparation of two-component host-guest samples. The host-guest samples with various molar ratio (100:0.1, 100:0.2, 100:0.5, 100:1, and 100:2) were prepared from a simple method of the evaporation of chloroform solution. For example, in the 100:0.5 sample, BTD(OMe)-Br (53.10 mg, 150 μmol) and BSeD(OMe)-Br (0.30 mg, 0.75 μmol) were dissolved in spectral grade chloroform (3 mL) and subsequently

evaporated in vacuo to dryness (ca. 150 torr/25 °C). Although the host-guest samples were prepared by also two different methods: the recrystallization method from chloroform/hexane and the melting method (150 °C, above melting point (133 °C) of BTD(OMe)-Br), the reproducible and reliable result was obtained from the evaporation method (Fig. S10).

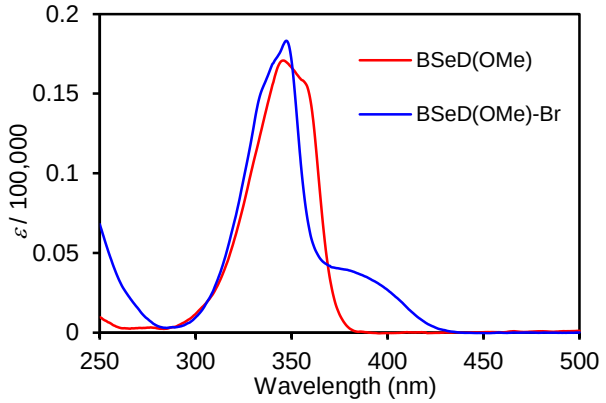

Fig. S1 UV/Vis absorption spectra of BSeD(OMe) and BSeD(OMe)-Br in DCM (1.0×10^{-5} M).

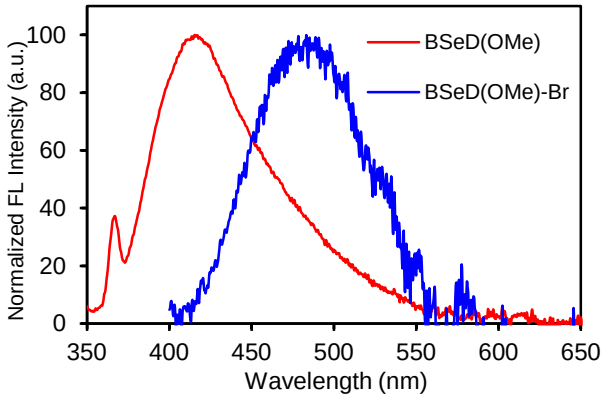

Fig. S2 Fluorescence spectra (ex. 330 nm) of BSeD(OMe) and BSeD(OMe)-Br in DCM (1.0×10^{-5} M).

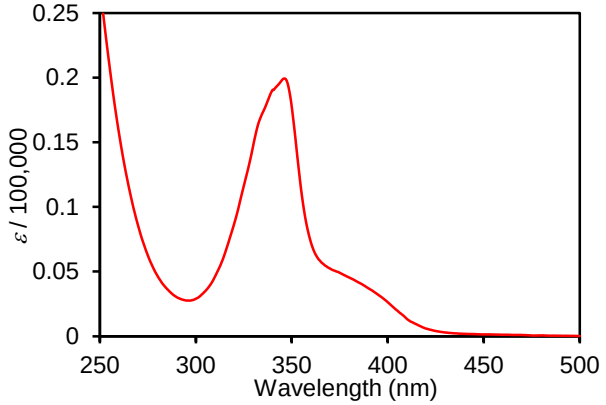

Fig. S3 UV/Vis absorption spectra of BSeD(OMe)-Br in THF (1.0×10^{-5} M).

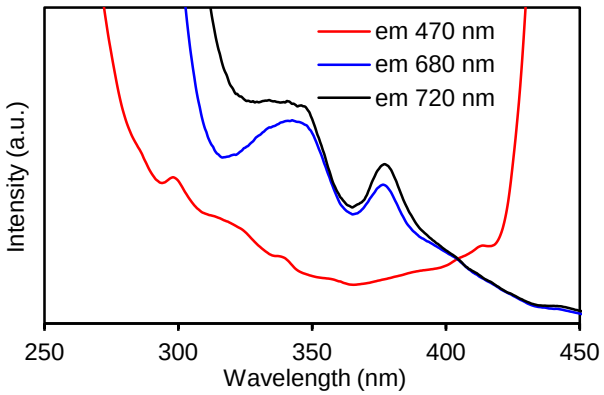

Fig. S4 Excitation spectra of BSeD(OMe)-Br monitored at 470, 680, and 720 nm in THF (1.0×10^{-5} M) at 77 K.

Table S1. Spectral data of BSeD(OMe) and BSeD(OMe)-Br in solution, [a]

Comp.	Solvent	λ_{abs} (nm)	ε	ex (nm)	λ_{em} (nm)	Φ_F (%) [b]	Φ_P (%) [b]
BSeD(OMe)	DCM	358 (sh)	15,280	330	415	0.09	
		346	16,880				
BSeD(OMe)-Br	DCM	385 (sh)	3,700	330	483	0.01	
		348	18,310				
		335 (sh)	15,390				
	THF	385 (sh)	4,150	350	474	0.01	
		346	19,930				
		335 (sh)	17,350				
	THF (77 K)	–	–	350	712	0.02	0.15
					660 (sh)		
					466		

[a] 1×10^{-5} M, [b] determined relative to quinine sulfate (Φ_{FL} 0.55, ex 350 nm) in sulfuric acid.

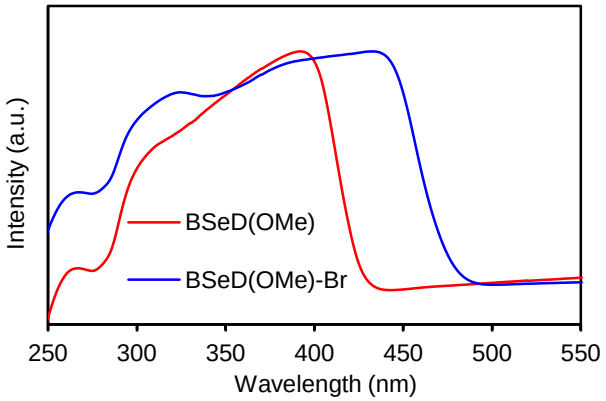

Fig. S5 Diffuse reflection UV/Vis spectra of BSeD(OMe) and BSeD(OMe)-Br in the crystalline solid state.

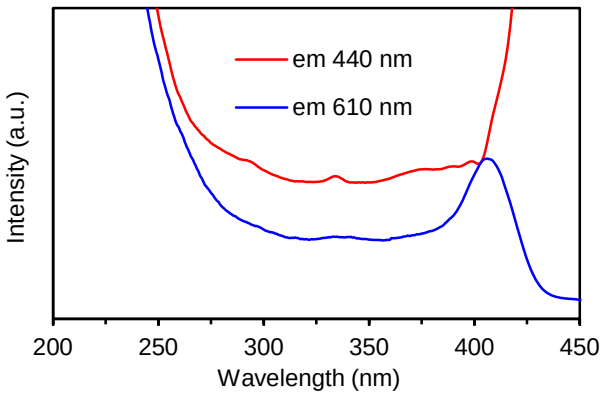

Fig. S6 Excitation spectra of BSeD(OMe) monitored at 440 and 610 nm in the crystalline solid state.

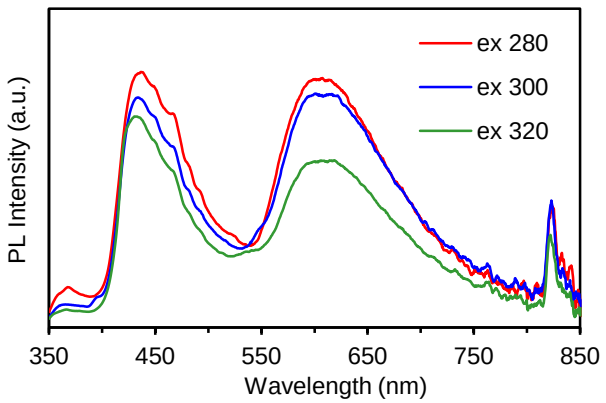

Fig. S7 Steady-state photoluminescence spectra (ex. 280, 300, and 320 nm) of BSeD(OMe) in the crystalline solid state.

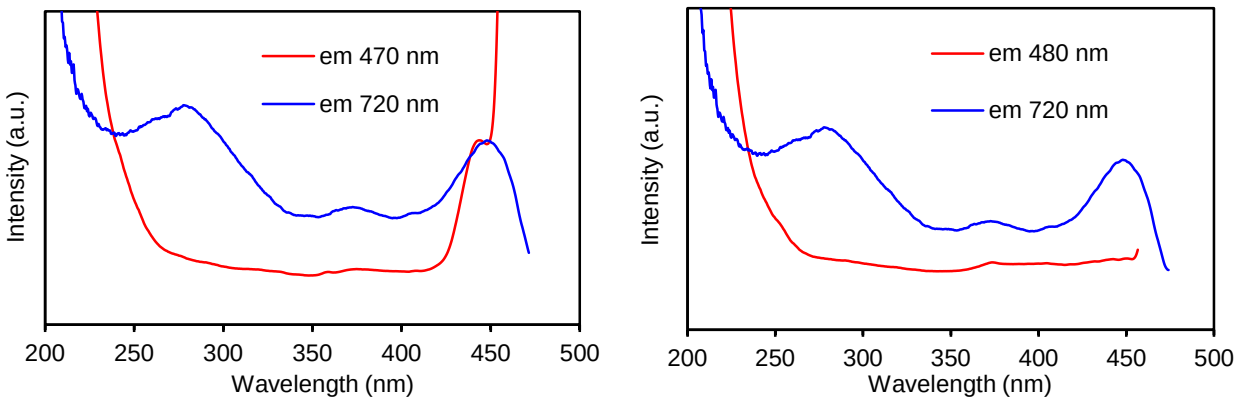

Fig. S8 Excitation spectra of BSeD(OMe)-Br monitored at 470 and 720 nm in the crystalline solid state.

In the crystalline solid state, the excitation spectral data is likely to support the intersystem crossing, starting from the higher-lying excited single. The monitoring of phosphorescence emission at 720 nm produces two excitation bands at 278 and 448 nm. The longer-wavelength excitation band at 448 nm is attributed to the transition from the ground state to the lowest excited singlet state, whereas the shorter-wavelength band at 278 nm is attributed to the transition to the higher-lying excited single. The shorter-wavelength excitation band was not observed in the monitoring of fluorescence emission at 470 nm. The observed shorter-wavelength band at 278 nm coincide with the finding that the excitation at 280 nm provided the maximum phosphorescence quantum yield (Fig. 2c).

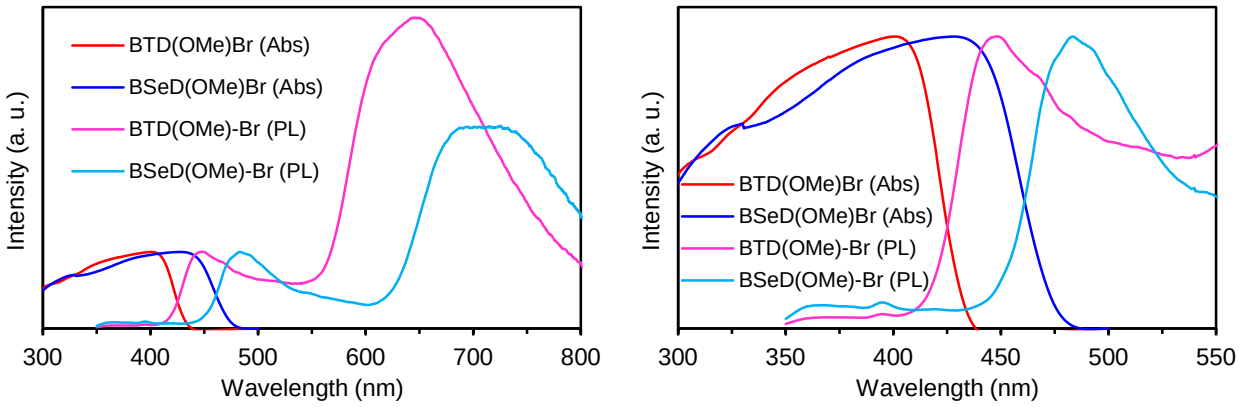

Fig. S9 Overlap plots of the diffuse reflection UV/Vis spectra and photoluminescence spectra (excited at 300 nm) of BTD(OMe)-Br and BSeD(OMe)-Br in the crystalline solid state. The right figure is an expansion of the overlap region between absorption and fluorescence bands.

The small overlap between fluorescence band of BTD(OMe)-Br and absorption band of BSeD(OMe)-Br indicates that Förster-type singlet-singlet energy-transfer is unfavored in this host–guest two-component system.

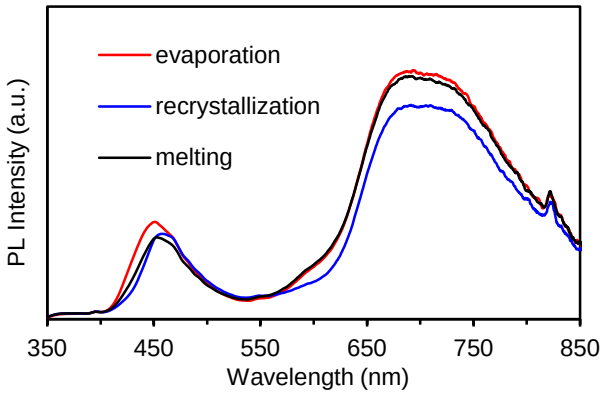

Fig. S10 Steady-state photoluminescence spectra (excited at 300 nm) of the mixture of BTD(OMe)-Br and BSeD(OMe)-Br (100:0.5 (mol/mol)) in the crystalline solid state. The mixture samples were prepared by different methods: the evaporation of chloroform solution, the recrystallization from chloroform/hexane, and the melting method (150 °C, above melting point (133 °C) of BTD(OMe)-Br).

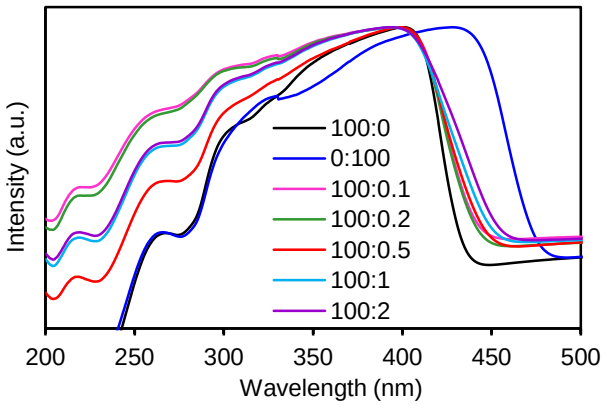

Fig. S11 Diffuse reflection UV/Vis spectra of the mixture of BTD(OMe)-Br and BSeD(OMe)-Br (100:0, 100:0.1, 100:0.2, 100:0.5, 100:1, 100:2, and 0:100 (mol/mol)) in the crystalline solid state.

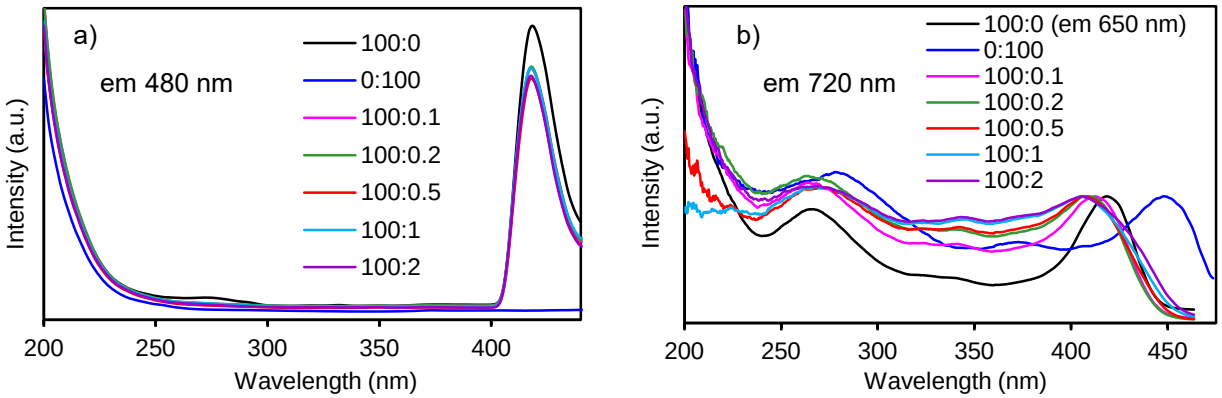

Fig. S12 Excitation spectra monitored at a) 480 nm and b) 720 nm for the mixture of BTD(OMe)-Br and BSeD(OMe)-Br (100:0, 100:0.1, 100:0.2, 100:0.5, 100:1, 100:2, and 0:100) in the crystalline solid state.

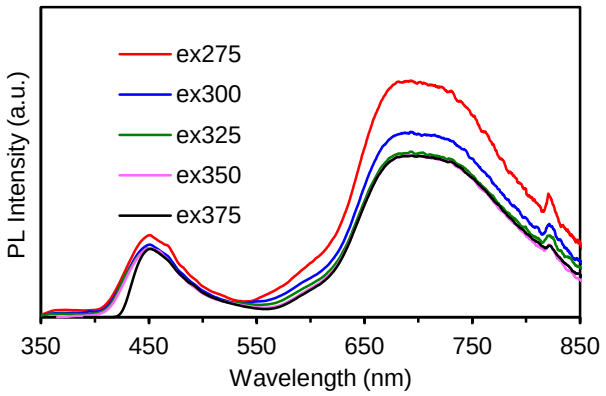

Fig. S13 Excitation dependence of steady-state photoluminescence spectra (excited at 275, 300, 325, 350, and 375 nm) of the mixture of BTD(OMe)-Br/BSeD(OMe)-Br (100:0.5 (mol/mol)) in the crystalline solid state.

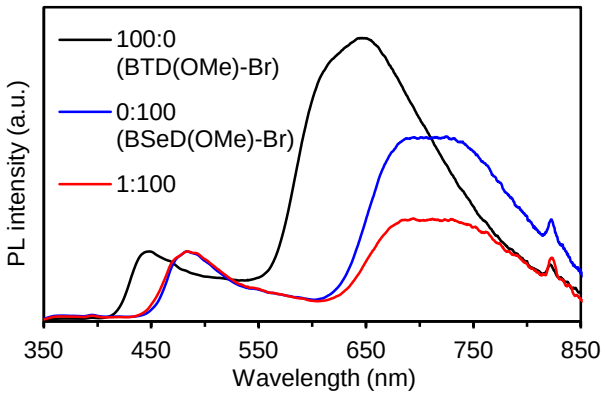

Fig. S14 Steady-state photoluminescence spectra (excited at 300 nm) of the mixture of BTD(OMe)-Br and BSeD(OMe)-Br (100:0, 0:100, and 1:100) in the crystalline solid state.

In the 1:100 sample, the fluorescence emission band (483 nm) of BSeD(OMe)-Br was remained. Judging from the this finding, the energy transfer from the singlet state of BSeD(OMe)-Br to the triplet state of BTD(OMe)-Br can be rejected.

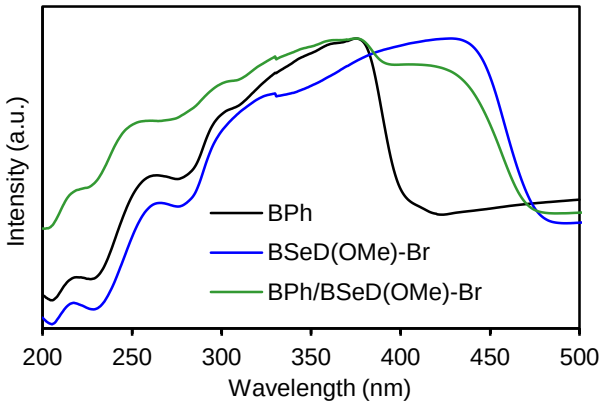

Fig. S15 Diffuse reflection UV/Vis spectra of BPh, BSeD(OMe)-Br, and BPh/BSeD(OMe)-Br (100:0.5) in the crystalline solid state.

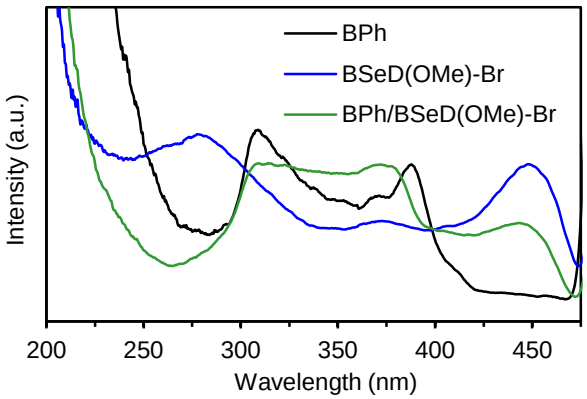

Fig. S16 Excitation spectra of BPh, BSeD(OMe)-Br, and BPh/BSeD(OMe)-Br (100:0.5 (mol/mol) (monitored at 700, 740, and 700 nm, respectively) in the crystalline solid state.

The mixture of BPh/BSeD(OMe)-Br sample exhibited the excitation band around 300–400 nm arising from the BPh absorption, suggesting the energy transfer from BPh to BSeD(OMe)-Br.

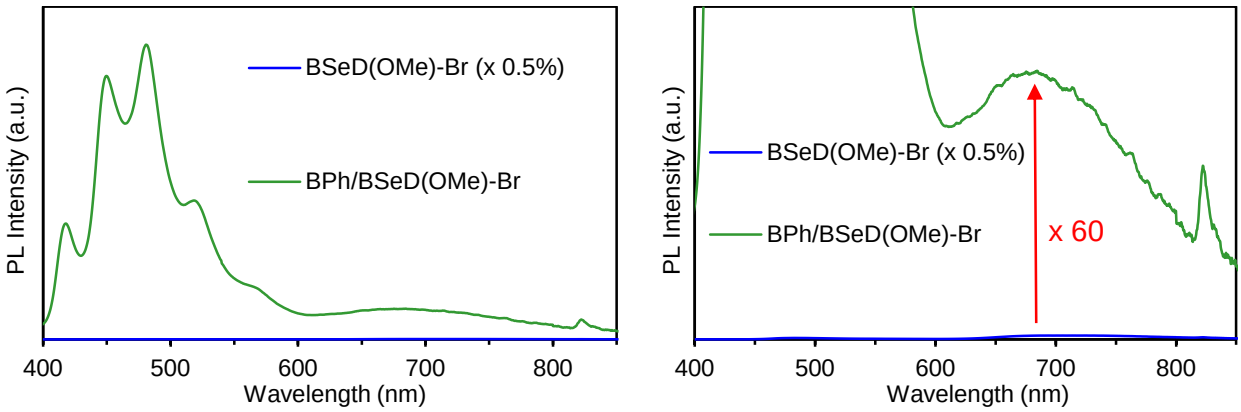

Fig. S17 Steady-state photoluminescence spectra (ex. 300 nm) of the mixture of BPh and BSeD(OMe)-Br (0:100 (× 0.5%) and 100:0.5) in the crystalline solid state.

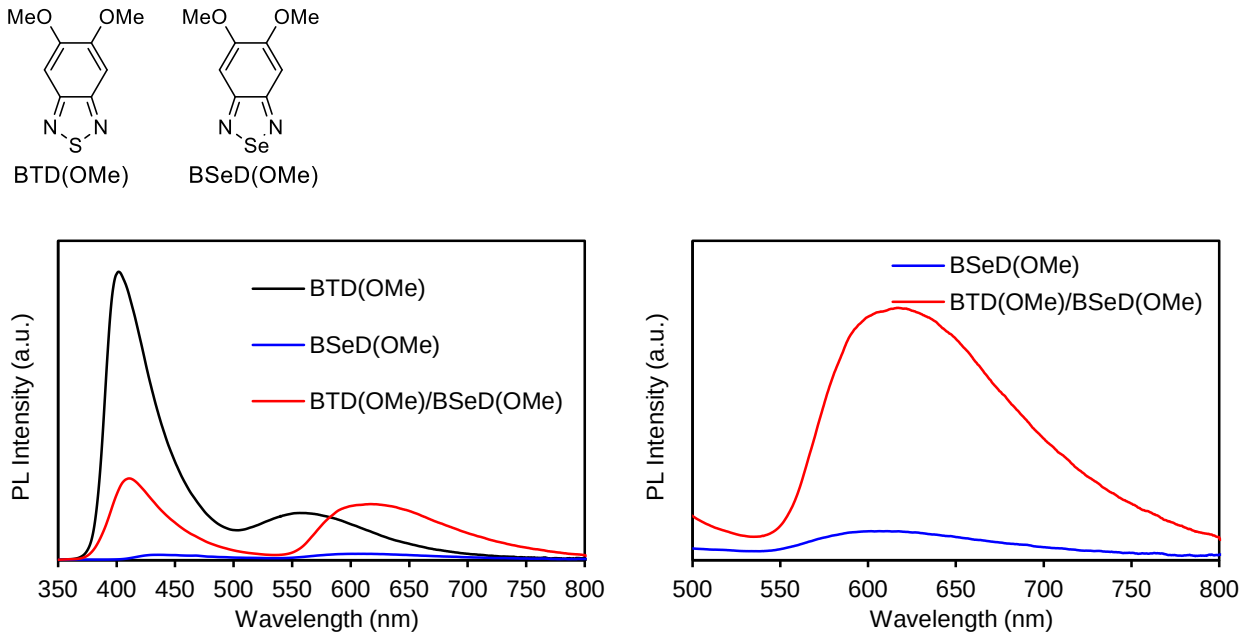

Fig. S18 Steady-state photoluminescence spectra (excited at 275 nm) of the mixture of BTD(OMe) and BSeD(OMe) (100:0.5) in the crystalline solid state: the right figure is an expansion of the phosphorescence bands in the single BSeD(OMe) and the mixture of BTD(OMe) and BSeD(OMe).

The present reference host–guest system indicated the disappearance of host phosphorescence emission at 555 nm and the appearance of guest phosphorescence emission at 618 nm, suggesting that the energy transfer works in this reference system without bromine atoms. Interesting, we found a strong phosphorescence enhancement by a factor of more than 1,000 (based on normalization of the molar ratio), together with the unpredictable bathochromic shits of phosphorescence (at 618 nm) and fluorescence emissions (at 410 nm). The detailed analysis will be reported elsewhere

Table S2 Spectral data of benzothiadiazole- and benzoselenodiazole-based dyes in the crystalline solid state,

Comp.	λ_{abs} (nm)	Fluorescence [a]				Phosphorescence [a]			
		λ_F (nm)	Φ_F (%) [b]	em (nm)	λ_{ex} (nm)	λ_P (nm)	Φ_P (%) [b]	em (nm)	λ_{ex} (nm)
BTD(OMe)-Br [c]	403 295(sh) 260(sh)	448	0.4	460	418	648	4.4	650	417 268
BSeD(OMe)	393 310 (sh) 268 218	437	0.4	440	399 391 378 334 296 293	608	0.4	610	406 333
BSeD(OMe)-Br	432 325 (sh) 267	483	0.2	470	444 374	ca. 720 (670–750)	1.4	720	448 371 278
(77 K)	–	469	0.4			743 684	1.9	–	–
BTD(OMe)-Br/ BSeD(OMe)-Br (100:0.1)	400 300 (sh) 260	449	0.4	460	418	673	2.1	720	412 265
(100:0.2)	400 300 (sh) 260	449	0.4	460	418	684	1.7	720	408 263
(100:0.5)	400 300 (sh) 260	451	0.4	460	418	ca. 720	1.5	720	406 264
(100:1)	400 300 (sh) 260	454	0.4	460	418	ca. 720	1.5	720	405 268
(100:2)	400 300 (sh) 260	458	0.4	460	418	ca. 720	1.5	720	405 270
(1:100)	415 320 262	483	–	–	–	ca. 720	–	–	–
BPh	375 300 264	–	–			518 481 447	11.0	480	390 370 313

						418			
BPh/	410	–	–	–	–	684	0.4	650	380
BSeD(OMe)-Br	375					518	(BSeD)		307
(100:0.5)	300					481			
	260					450	2.0	480	382
						418	(BPh)		312

[a] excited at 300 nm, [b] absolute fluorescence and phosphorescence quantum yields determined by an integrating sphere system, [c] reported data: T. Ishi-i, R. Kichise, I. S. Park, T. Yasuda and T. Matsumoto, *J. Mater. Chem. C*, 2023, **11**, 3003–3009.

Table S3 Fluorescence and phosphorescence quantum yields of benzothiadiazole- and benzoselenodiazole-based dyes in the crystalline solid state,

Comp.	Conditions	Ex. (nm)	Φ_F (%) [a]	Φ_P (%) [a]
BTD(OMe)-Br [b]	r.t.	350	0.4	3.0
		325	0.4	3.7
		300	0.4	4.4
		270	0.4	6.9
BSeD(OMe)	r.t.	320	0.3	0.3
		300	0.4	0.4
		280	0.4	0.4
BSeD(OMe)-Br	r.t.	350	0.3	0.8
		340	0.3	0.8
		320	0.3	1.0
		300	0.4	1.4
		280	0.4	1.6
		260	0.5	1.5
	77 K	280	0.4	1.9
BTD(OMe)-Br/	100:0.1	350	0.4	1.8
BSeD(OMe)-Br	r.t.	300	0.4	2.1
	100:0.2	350	0.4	1.5
	r.t.	300	0.4	1.7
	100:0.5	375	0.4	1.3
	r.t.	350	0.4	1.3
		325	0.4	1.4
		300	0.4	1.5
		275	0.5	2.0
	100:1	350	0.4	1.3
	r.t.	300	0.4	1.5
	100:2	350	0.4	1.3
	r.t.	300	0.4	1.5
BPh/	100:0.5	350		0.4 (BSeD)
BSeD(OMe)-Br	r.t.			1.4 (BPh)
		300		0.4 (BSeD)
				2.0 (BPh)
		275		0.3 (BSeD)
				1.4 (BPh)

[a] absolute fluorescence and phosphorescence quantum yields determined by an integrating sphere system, [b] reported data: T. Ishi-i, R. Kichise, I. S. Park, T. Yasuda and T. Matsumoto, *J. Mater. Chem. C*, 2023, **11**, 3003–3009.

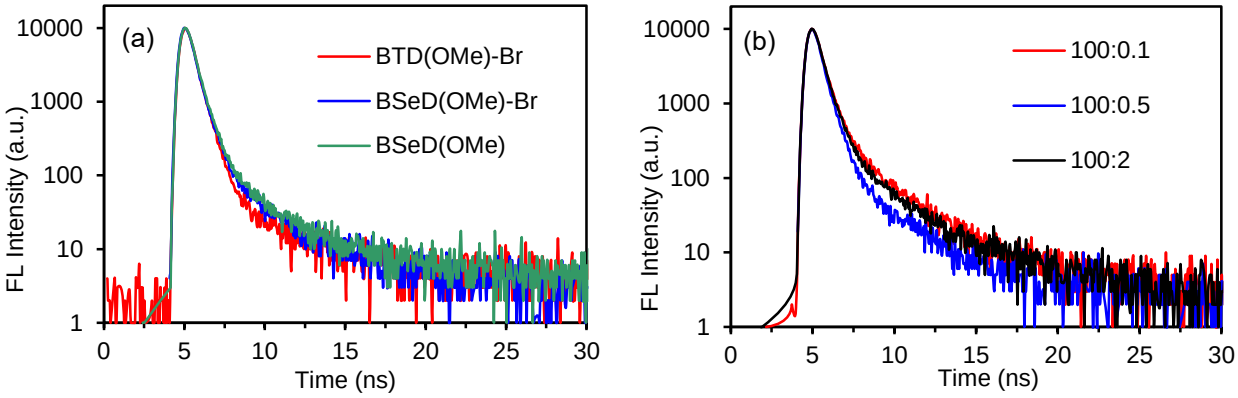

Fig. S19 Fluorescence decay curves of (a) BSeD(OMe)-Br, BSeD(OMe)-Br, and BSeD(OMe) (monitored at 450, 480, and 400 nm, respectively) and (b) the mixture of BTD(OMe)-Br and BSeD(OMe)-Br (100:0.1, 100:0.5, and 100:2 (mol/mol)) (monitored at 480 nm) with excitation at 340 nm in the crystalline solid state. Experimental decay curves are fitted with a double-exponential function.

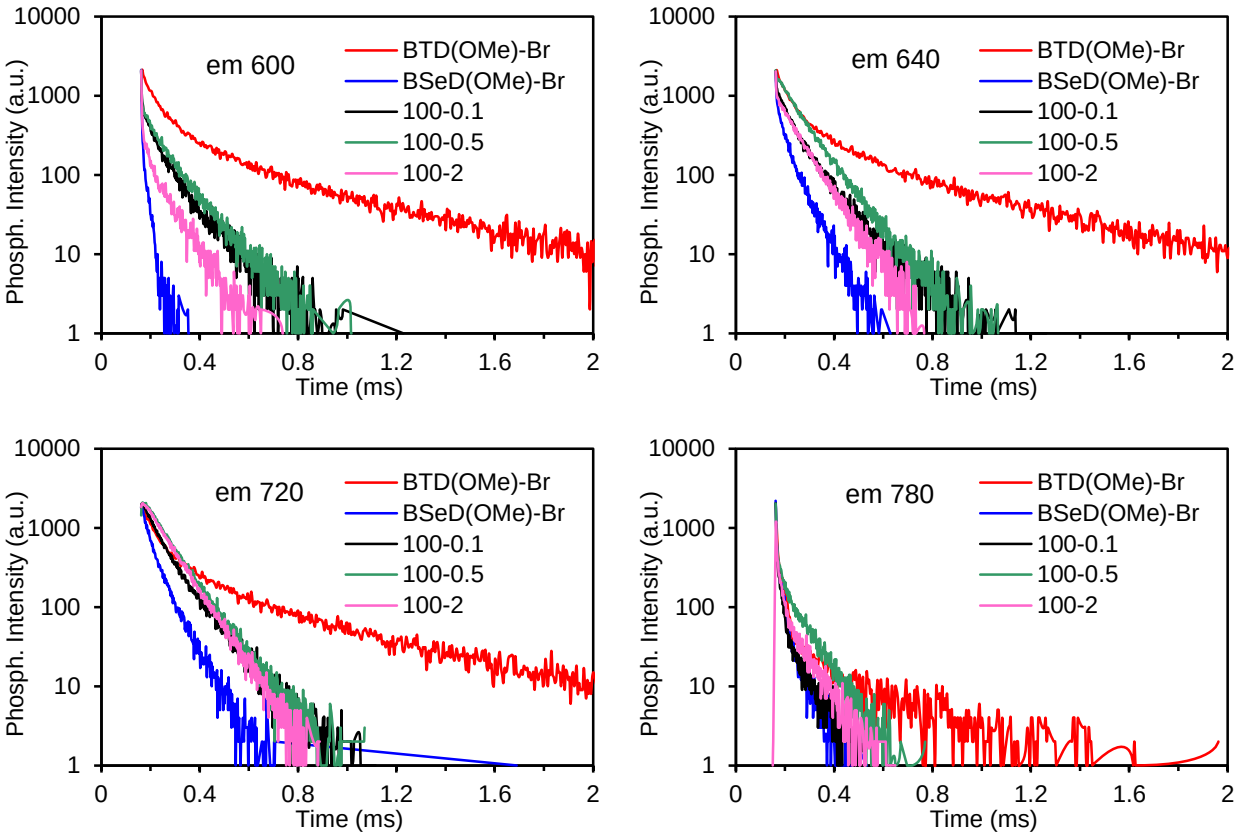

Fig. S20 Phosphorescence decay curves (monitored at 600, 640, 720, and 780 nm) of the mixture of BTD(OMe)-Br and BSeD(OMe)-Br (100:0, 0:100, 100:0.1, 100:0.5, and 100:2 (mol/mol)) in the crystalline solid state with excitation at 340 nm. Experimental decay curves are fitted with a triple-exponential function.

The energy-transfer efficiency Φ_{EN} was calculated from the equation (1):

$$\Phi_{EN} = 1 - \tau_{(H\text{-}G)} / \tau_{(H)} \quad (1)$$

$\tau_{(H\text{-}G)}$ and $\tau_{(H)}$ are phosphorescence lifetime of host-guest and host, respectively. In the single guest BSeD(OMe)-Br, the phosphorescence lifetime was given to be 63 μs. Thus, this value was used as a standard of energy transfer efficiency of 100%. Based on the phosphorescence lifetime change (em. 640 nm), the energy transfer efficiency Φ_{EN} was calculated to be 92% (100:0.5) and 95% (100:2).

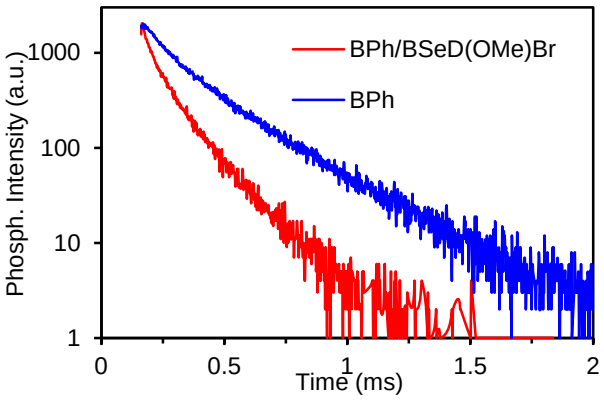

Fig. S21 Phosphorescence decay curves (monitored at 450 nm) of BPh and BPh/BSeD(OMe)Br (100:0.5 (mol/mol)) with excitation at 340 nm.

The energy-transfer efficiency Φ_{EN} was calculated from the equation (1):

$$\Phi_{EN} = 1 - \tau_{(H\text{-}G)} / \tau_{(H)} \quad (1)$$

$\tau_{(H\text{-}G)}$ and $\tau_{(H)}$ are phosphorescence lifetime of host-guest and host, respectively. Based on the phosphorescence lifetime change (450 nm), the energy-transfer efficiency Φ_{EN} was calculated to be 43%.

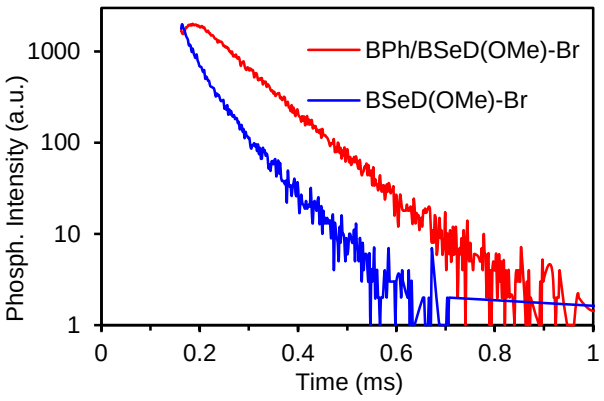

Fig. S22 Phosphorescence decay curves (monitored at 720 nm) of BPh/BSeD(OMe)Br (100:0.5 (mol/mol)) and BSeD(OMe)-Br with excitation at 340 nm.

Table S4 Fluorescence and phosphorescence lifetime data of benzothiadiazole- and benzoselenodiazole-based dyes in the crystalline solid state,

Comp.	Fluorescence [a]				Phosphorescence [a]			
	Φ_F (%) [b]	em (nm)	τ_F (ns) (f_i (%)) [c]	$<\tau_F>$ (ns) [d]	Φ_P (%) [b]	em (nm)	τ_P (μs) (f_i (%)) [c]	$<\tau_P>$ (μs) [d]
BTD(OMe)-Br [e]	0.4	450	0.10 (98) 4.58 (2)	2.32	3.7	600	7.65 (9) 88.9 (38) 529.7 (53)	482
						640	12.2 (11) 101.1 (38) 552.8 (51)	497
						720	13.2 (13) 107.3 (37) 557.4 (50)	499
						780	1.34 (41) 17.6 (26) 173.3 (33)	160
BSeD(OMe)	0.3	440	0.07 (96) 3.48 (4)	2.42	0.3	610	0.84 (26) 14.1 (47) 73.7 (27)	58
BSeD(OMe)-Br	0.4	480	0.01 (82) 2.37 (18)	2.67	0.8	600	0.03 (22) 25.2 (78)	25
						640	0.63 (14) 15.2 (27) 67.9 (59)	63
						720	1.59 (7) 14.4 (29) 66.4 (64)	62
						780	0.63 (42) 9.99 (28) 51.3 (29)	44
BTD(OMe)-Br/ BSeD(OMe)-Br (100:0.1)	0.5	450	0.01 (82) 2.37 (18)	2.67	1.8	600	0.28 (5) 31.5 (27) 105.6 (68)	98
						640	0.67 (5) 32.8 (27) 109.0 (68)	101
						720	1.39 (3)	98

							35.4 (27) 105.4 (70)	
						780	0.57 (41) 12.3 (28) 71.7 (31)	63
(100:0.5)	0.4	450	0.06 (96) 3.36 (4)	2.34	1.3	600	0.42 (6) 31.4 (13) 106.0 (81)	103
						640	0.69 (2) 30.2 (10) 99.7 (88)	98
						720	1.49 (1) 50.0 (18) 102.1 (81)	97
						780	0.68 (23) 12.2 (13) 81.5 (64)	79
(100:2)	0.4	450	0.01 (85) 2.76 (15)	2.69	1.3	600	0.40 (20) 17.4 (7) 76.9 (73)	76
						640	0.56 (6) 33.8 (8) 89.2 (86)	87
						720	0.96 (2) 33.4 (6) 90.7 (92)	89
						780	0.58 (31) 11.4 (19) 74.6 (50)	71
BPh	–	–	–	–		450	3.2 (1) 84.4 (20) 241.7 (79)	229
						480	2.8 (0.1) 91.0 (23) 253.2 (77)	237
BPh/ BSeD(OMe)-Br (100:0.5)	–	–	–	–	1.4	450 (BPh)	5.4 (11) 43.6 (26) 143 (63)	131
						480	3.9 (8)	134

		(BPh)	49.9 (32)	
			150 (60)	
	0.3	720	92 (100)	92
		(BSeD)		

[a] excited at 340 nm, [b] absolute fluorescence and phosphorescence quantum yields determined by an integrating sphere system, [c] the value in parentheses is the fractional contribution of component i to the total steady-state intensity, which was calculated by $f_i = (A_i \tau_{Fi}/\Sigma A_i \tau_{Fi}) \times 100$, [d] The intensity-averaged decay lifetime ($<\tau>$) was calculated as follows: $<\tau> = \Sigma(A_n \tau_n^2)/\Sigma(A_n \tau_n)$, in which A_n is the coefficient of each exponential term, [e] although the lifetime (em. 640 nm) of BTD(OMe)-Br was reported already in the reference (T. Ishi-i, R. Kichise, I. S. Park, T. Yasuda and T. Matsumoto, *J. Mater. Chem. C*, 2023, **11**, 3003–3009), the present lifetime was measured newly.

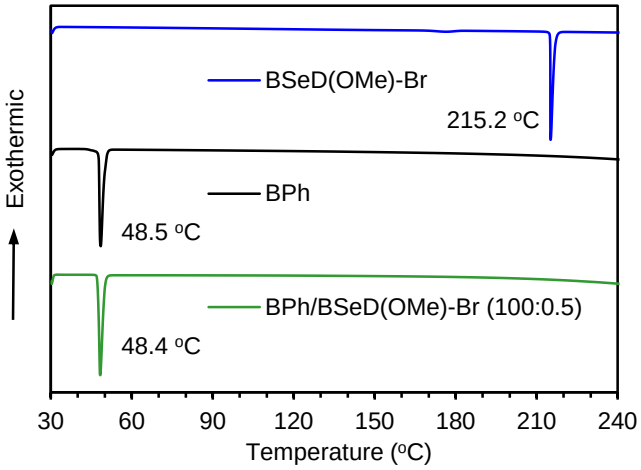

Fig. S23 DSC traces of BSeD(OMe)-Br, BPh, and BPh//BSeD(OMe)-Br (100:0.5 (mol/mol)) in the crystalline solid state.

Table S5 Thermal analysis data obtained from DSC traces of BTD(OMe)-Br, BSeD(OMe)-Br, and BPh dyes.

Sample	T_m/°C (ΔH/kJ mol^{-1})
BTD(OMe)Br	132.9 (–25.1)
BSeD(OMe)-Br	215.2 (–32.1)
BTD(OMe)-Br/BSeD(OMe)-Br (100:0.5, (mol/mol))	134.1 (–25.8)
BTD(OMe)-Br/BSeD(OMe)-Br (100:2, (mol/mol))	135.5 (–25.4)
BPh	48.5 (–19.1)
BPh/BSeD(OMe)-Br (100:0.5, (mol/mol))	48.4 (–18.8)

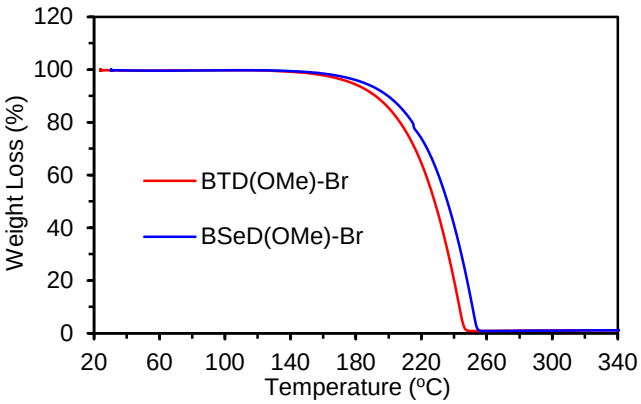

Fig. S24 TGA traces of BTD(OMe)-Br and BSeD(OMe)-Br.

The weight loss was started at around 200 °C both in BTD(OMe)-Br (10% weight loss: ca.192 °C) and BSeD(OMe)-Br (10% weight loss: ca. 215 °C). The thermal analysis indicated that in the host-guest system the guest BSeD(OMe)-Br molecule is stale in the melting process (ca. 133 °C) of the guest molecule.

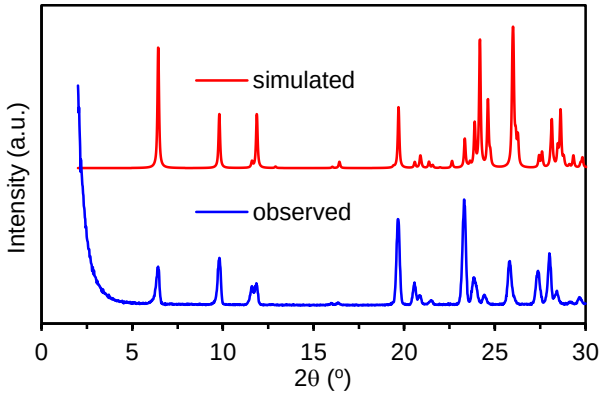

Fig. S25 Powder XRD patterns of BSeD(OMe)-Br in the crystalline solid state and the simulated powder pattern derived from a single crystal.

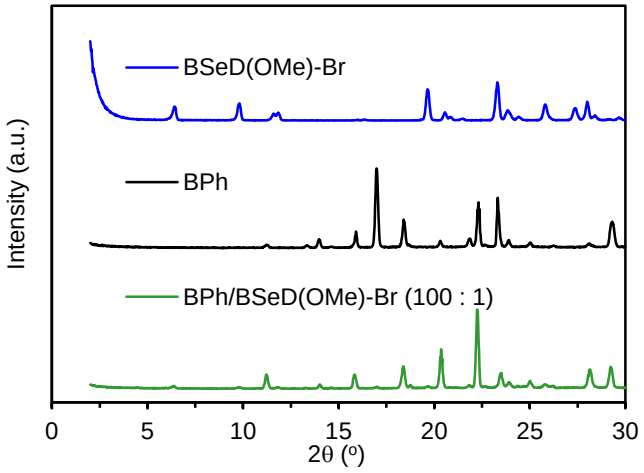

Fig. S26 Powder XRD patterns of BSeD(OMe)-Br, BPh, and BPh//BSeD(OMe)-Br (100:0.5 (mol/mol)) in the crystalline solid state.

Computer simulation analysis.

All quantum chemical calculations based on the time-dependent density functional theory (TD-DFT) were performed using the ADF2023 program package.[1] The ground-state (S_0) geometries for the compound BTD(OMe)-Br were initially optimized using the B3LYP functional with the DZP basis set in the gas phase. The vertical excitation calculations were carried out using the optimized S_0 geometries, and the geometry optimizations in the excited S_1 and T_1 states were performed using TD-DFT at the same level of theory. For the $S_0 \rightarrow S_m$ (m = 1−4) and $S_0 \rightarrow T_n$ (n = 1−4) transitions, the natural transition orbitals (NTOs) with their excitation energies were simulated using the optimized S_1 and T_1 geometries, respectively. Using the T_1 geometries, the spin−orbit coupling matrix elements, $\langle S_m|\hat{H}_{SOC}|T_n\rangle$, were calculated using a scalar relativistic TD-DFT with the two-component zeroth-order relativistic approximation (ZORA)[2] at the same level of theory. The contributions of the three degenerate triplet states ($T_{n,x}$, $T_{n,y}$, and $T_{n,z}$) were taken into account by calculating the root sum square of the real and imaginary parts (Re and Im, respectively) of the matrix elements, as expressed by the following equation:[3]

$$\langle S_m|\hat{H}_{SOC}|T_n\rangle = \{\sum_{a=x,y,z}(\mathrm{Re}^2\langle S_m|\hat{H}_{SOC}|T_{n,a}\rangle + \mathrm{Im}^2\langle S_m|\hat{H}_{SOC}|T_{n,a}\rangle)\}^{1/2}$$

1 ADF2023, SCM, Theoretical Chemistry, Vrije Universiteit, Amsterdam, The Netherlands, http://www.scm.com/.

2 F. Wang and T. Ziegler, *J. Chem. Phys.*, 2005, **123**, 154102.

3 E. Y.-T. Li, T.-Y. Jiang, Y. Chi and P.-T. Chou, *Phys. Chem. Chem. Phys*., 2014, **16**, 26184–26192.

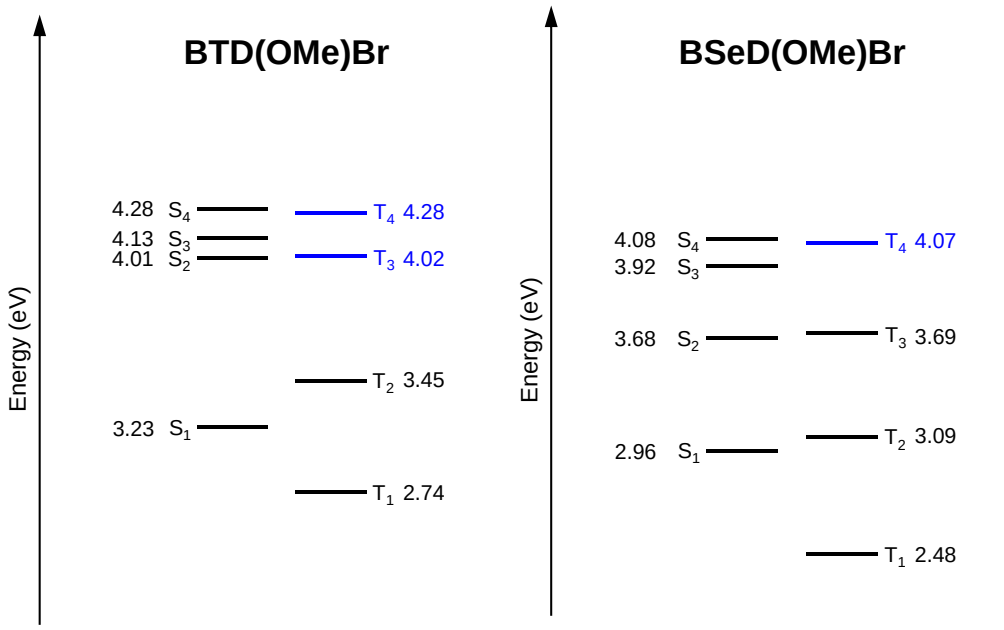

SOCME $\langle S_n|\hat{H}_{SOC}|T_m\rangle$

	T_1	T_2	T_3	T_4
S_1	3.39	13.76	654.03	96.01
S_2	508.95	18.08	9.39	191.85
S_3	225.97	10.36	22.70	256.93
S_4	74.95	118.13	168.83	47.54

SOCME $\langle S_n|\hat{H}_{SOC}|T_m\rangle$

	T_1	T_2	T_3	T_4
S_1	2.23	1.10	574.26	58.60
S_2	488.10	151.32	22.93	60.39
S_3	80.78	26.96	137.34	114.08
S_4	60.99	93.62	113.28	601.61

Fig. S27 Theoretical calculated energy diagram and spin−orbit coupling matrix elements (SOCME) of BTD(OMe)-Br and BSeD(OMe)-Br.

In BSeD(OMe)-Br, a favored intersystem crossing in S_3/T_3, S_3/T_4, S_4/T_3 and S_4/T_4 was indicated by higher SOCME values of 137.34, 114.08, 113.28, and 601.61 cm^{-1}, respectively, together with small band gap within 0.39 eV. The large energy gap (>0.96 eV) between S_1 and S_3/S_4 is supportive of the intersystem crossing starting from higher-lying S_3/S_4, because the internal conversion from S_3/S_4 to S_1 is slow.

Although the theoretical calculation of BTD(OMe)-Br was already done in the previous study (ADF2019), the present calculation has been performed newly using the new ADF2023 program package.

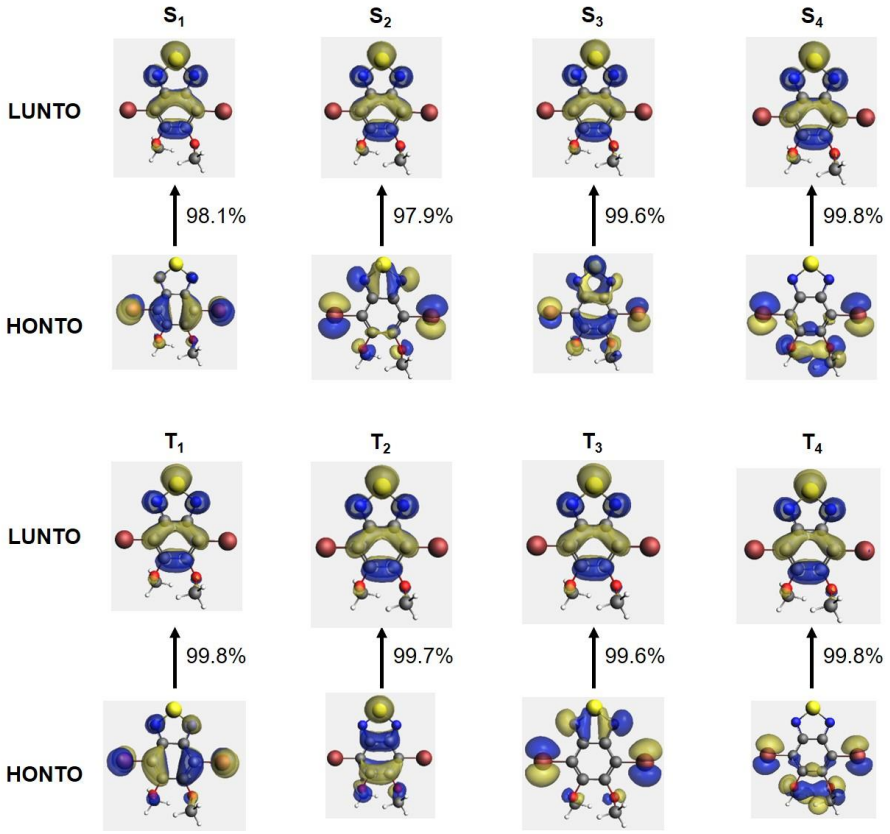

Fig. S28 Theoretical calculated natural transition orbitals (HONTOs and LUNTOs) of BTD(OMe)-Br.

According to El-Sayed rule, the S_1/T_2 intersystem crossing is unfavored, because both the S_1 and T_2 states can be assigned to the same configuration of π/π^* transition. In contrast, the intersystem crossing in S_2/T_4 and S_3/T_4 is likely to be favored because of the contribution of both π/π^* and n/π^* configurations.

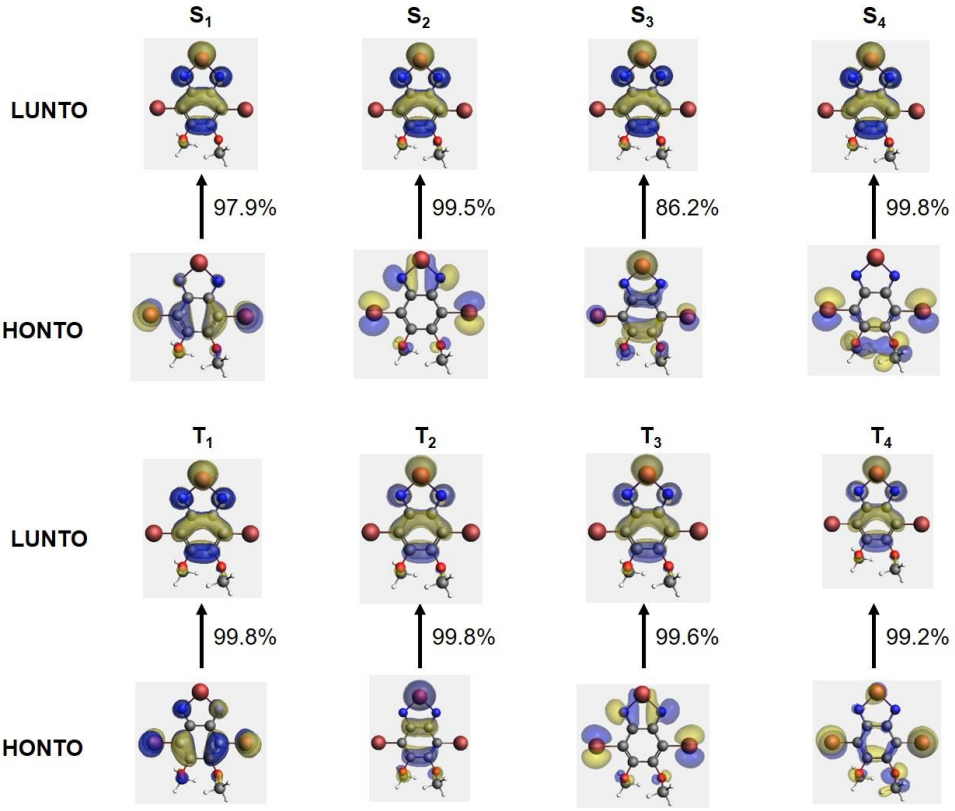

Fig. S29 Theoretical calculated natural transition orbitals (HONTOs and LUNTOs) of BSeD(OMe)-Br.

According to El-Sayed rule, the S_1/T_2 intersystem crossing is unfavored, because both the S_1 and T_2 states can be assigned to the same configuration of π/π^* transition. In contrast, the intersystem crossing in S_3/T_3, S_3/T_4, S_4/T_3 and S_4/T_4 is likely to be favored because of the contribution of both π/π^* and n/π^* configurations.

Single crystal X-ray diffraction analysis.

The single crystals for the X-ray diffraction analysis were obtained by the slow diffusion of hexane into the chloroform solution in BSeD(OMe)-Br (pale yellow needles).

All measurements were made on a Rigaku XtaLAB Synergy R/DW diffractometer coupled to a Rigaku AFC HyPix-6000 detector with Mo Kα radiation (λ = 0.71073 Å). Using Olex2,[1] the structure was solved with the Olex2.solve[2] structure solution program using Charge Flipping and refined with the Olex2.refine[2] refinement package using Gauss-Newton minimization. The non-hydrogen atoms were refined anisotropically. Hydrogen atoms were refined using the riding model. Simulated powder patterns were generated with Mercury 4.2 from the structures determined by single crystal diffraction analyses.[3]

1 O. V. Dolomanov, L. J. Bourhis, R. J. Gildea, J. A. K. Howard and H. Puschmann, OLEX2: A complete structure solution, refinement and analysis program. *J. Appl. Cryst.*, 2009, **42**, 339–341.

2 L. J. Bourhis, O. V. Dolomanov, R. J. Gildea, J. A. K. Howard and H. Puschmann, *Acta Cryst*., 2015, **A71**, 59–75.

3 https://www.ccdc.cam.ac.uk/support-and-resources/Downloads/

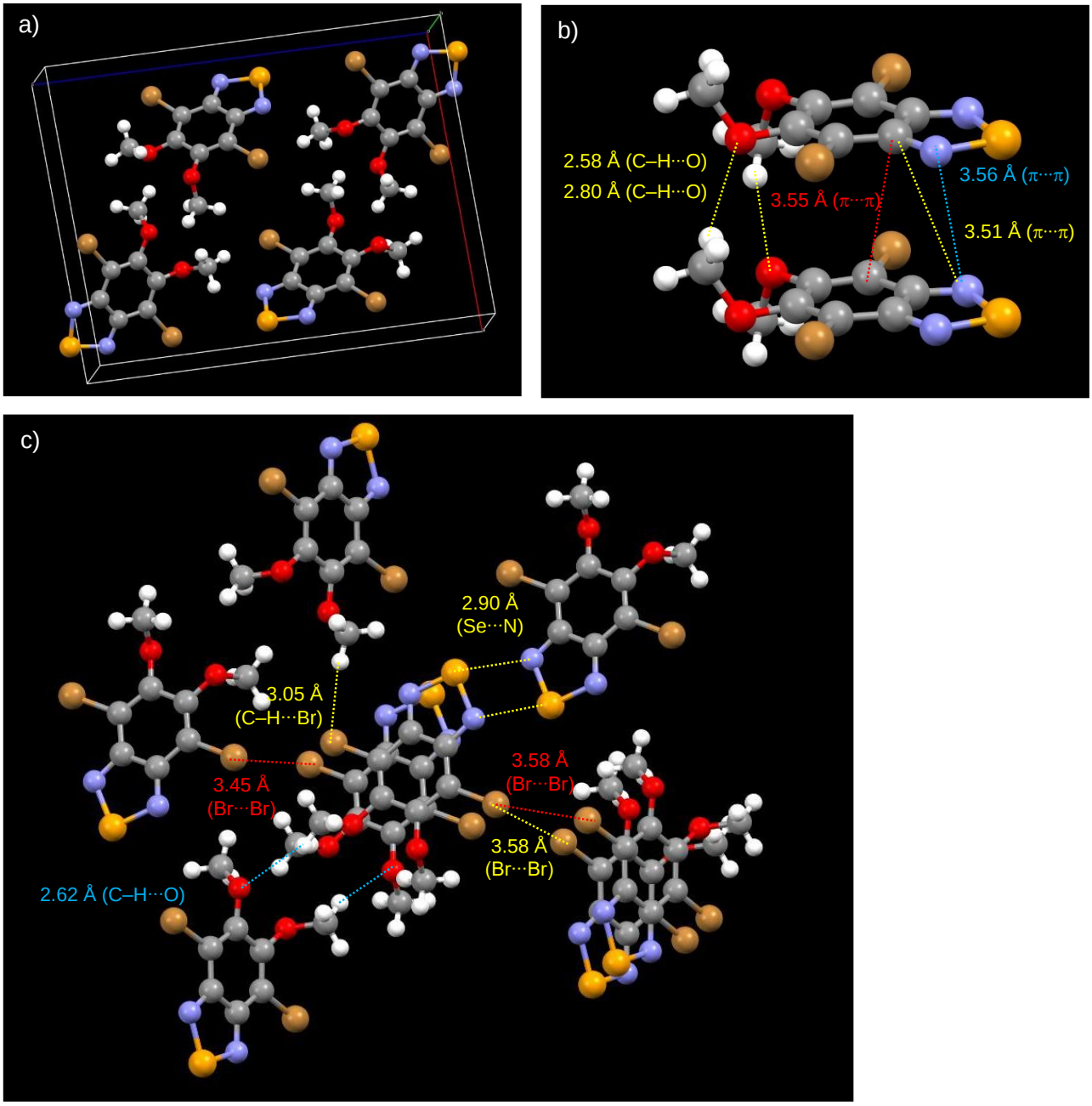

Fig. S30 Single crystal X-ray structure of BSeD(OMe)-Br: a) unit cell packing, b) dimeric structure in the one-dimensional columnar structure (shown in Fig. 3 in the manuscript), and c) intermolecular non-bonded interactions around the dimeric structure (shown in Fig. S30b).

The dimeric structure constructed by π···π stacking interactions is assisted by the two-point C–H···O interactions. The inter-columnar structure is stabilized by the multiple non-bonded interactions including halogen interactions, leading to an acceleration of ISC and the subsequent stabilization of excited triplet state.

Table S6 Selected data for the single crystals of BTD(OMe)-Br and BSeD(OMe)-Br dyes,

data		BTD(OMe)-Br [a]	BSeD(OMe)-Br
Monomer:			
molecular symmetry		asymmetry	asymmetry
bond length (Å)	C–Br	1.874, 1.874	1.881, 1.882
	C–O	1.363, 1.369	1.367, 1.373
dihedral angle (°)	BTD–OMe	85.3, 101.1	90.9, 92.1
Stacked dimer:			
intermolecular interactions (Å)	BTD···BTD (π···π)	3.518, 3.528, 3.553 (×2),	3.512, 3.552, 3.564 (×2)
(torsion angel (°))	OMe···OMe (C–H···O)	2.600 (149.5) (×2), 2.786 (161.9) (×2),	2.582 (148.6) (×2), 2.797 (164.8) (×2),
Packing:			
intermolecular interactions (Å) (torsion angel (°))	Br interactions	3.416 (Br···Br), 3.575 (Br···Br), 3.575 (Br···Br), 3.103 (146.1) (C–H···Br) (×2)	3.453 (Br···Br), 3.588 (Br···Br), 3.588 (Br···Br), 3.051 (148.8) (C–H···Br) (×2)
	N/S interactions	3.089 (N···S) (×2)	2.903 (N···Se) (×2)
	others	2.612 (164.4) (C–H···O) (×2)	2.624 (160.7) (C–H···O) (×2)
Intermolecular interaction point		19	19

[a] reported data: T. Ishi-i, R. Kichise, I. S. Park, T. Yasuda and T. Matsumoto, *J. Mater. Chem. C*, 2023, **11**, 3003–3009.

Table S7 Crystallographic data for BTD(OMe)-Br and BSeD(OMe)-Br dyes,

	BTD(OMe)-Br [a]	BSeD(OMe)-Br
CCDC number	2234914	2373646
formula	$C_8H_6Br_2N_2O_2S$	$C_8H_6Br_2N_2O_2Se$
M	354.03	400.93
T [K]	100	100
crystal system	monoclinic	monoclinic
space group	$P2_1/c$ (no. 14)	$P2_1/c$ (no. 14)
a [Å]	13.7002 (7)	13.6998 (2)
b [Å]	4.3371 (2)	4.35670 (10)
c [Å]	17.9709 (8)	18.0116 (3)
α [°]	90	90
β [°]	90.883 (4)	91.419 (2)
γ [°]	90	90
V [Å^3]	1067.69 (9)	1074.71 (3)
Z	4	4
ρ_{calcd} [g cm^{-3}]	2.202	2.478
μ [mm^{-1}]	7.767 (MoKα)	13.316 (MoKα)
F (000)	680	752
crystal size [mm^3]	0.3 × 0.1 × 0.02	0.21 × 0.07 × 0.05
θ range [°]	2.27–27.5	3.23–79.26
index range	–16 17	–16 17
	–5 5	–5 3
	–22 23	–22 22
reflections collected	8878	8169
reflections unique	2420	2299
R_{int}	0.0427	0.0282
data [$F^2 > 2\sigma(F^2)$]	2170	2196
parameters	138	138
goodness-of-fit	1.074	1.099
$R1/wR^2$ [$F^2 > 2\sigma(F^2)$]	0.0303/0.0696	0.0291/0.0809
$R1/wR^2$ (all data)	0.0361/0.0718	0.0304/0.0822
Resd. min/max [eÅ^{-3}]	–0.71/0.78	–1.12/0.79
Max Shift/error in final cycle	0.001	0.001

[a] reported data: T. Ishi-i, R. Kichise, I. S. Park, T. Yasuda and T. Matsumoto, *J. Mater. Chem. C*, 2023, **11**, 3003–3009.

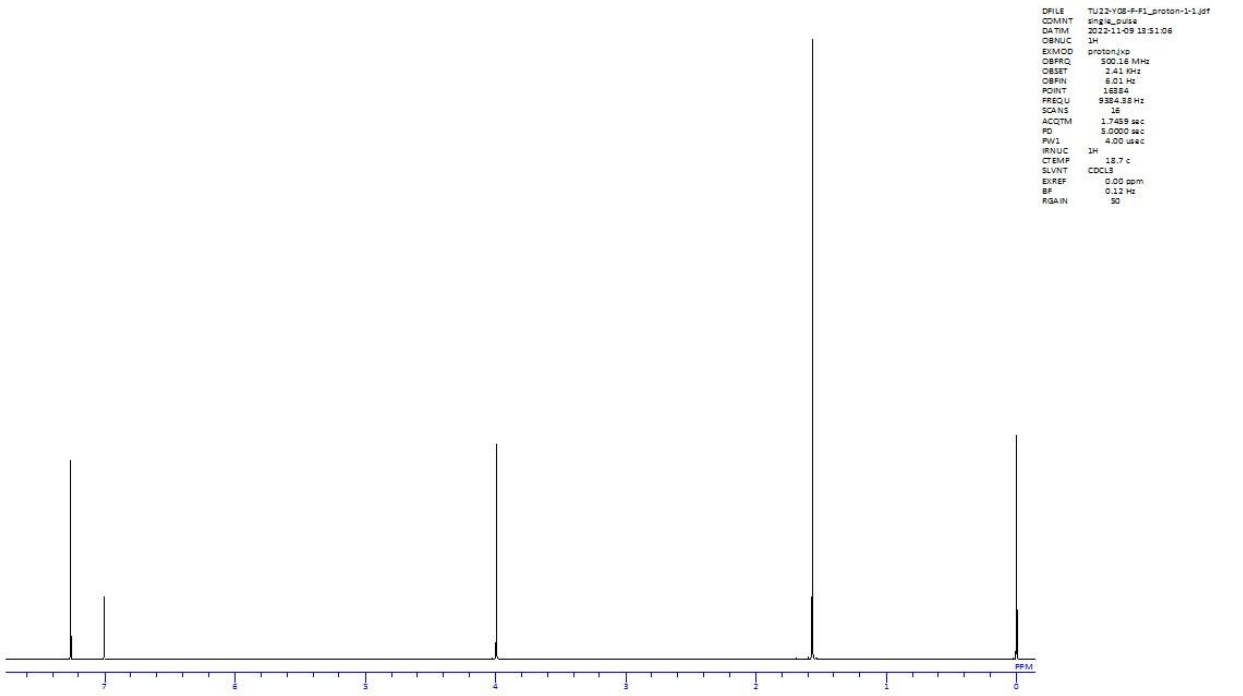

Fig. 31 ^{1}H NMR spectrum of BSeD(OMe) in $CDCl_3$ at room temperature.

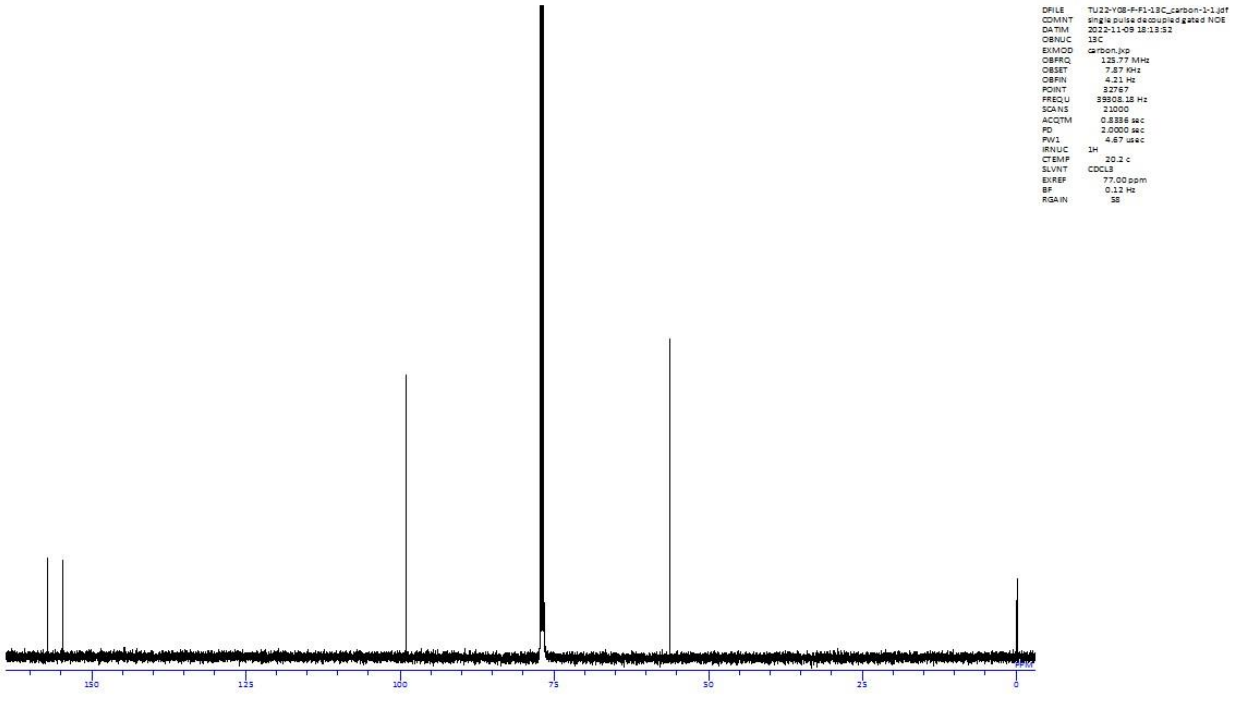

Fig. 32 ^{13}C NMR spectrum of BSeD(OMe) in $CDCl_3$ at room temperature.

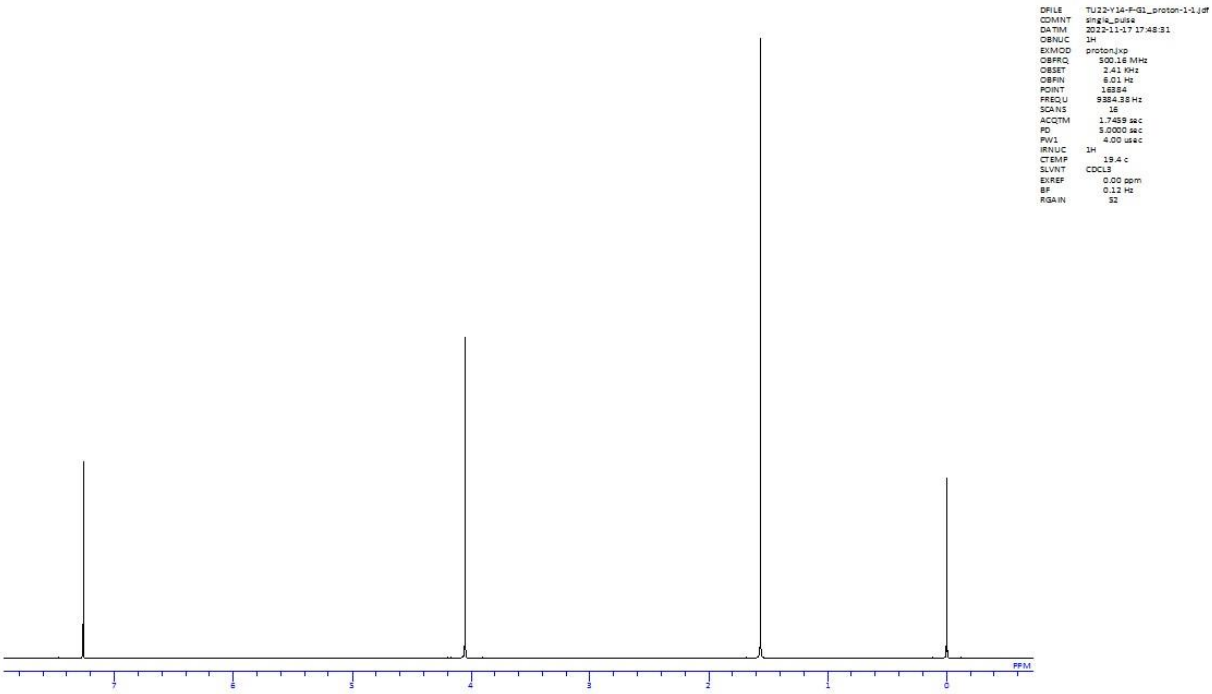

Fig. 33 ^{1}H NMR spectrum of BSeD(OMe)-Br in $CDCl_3$ at room temperature.

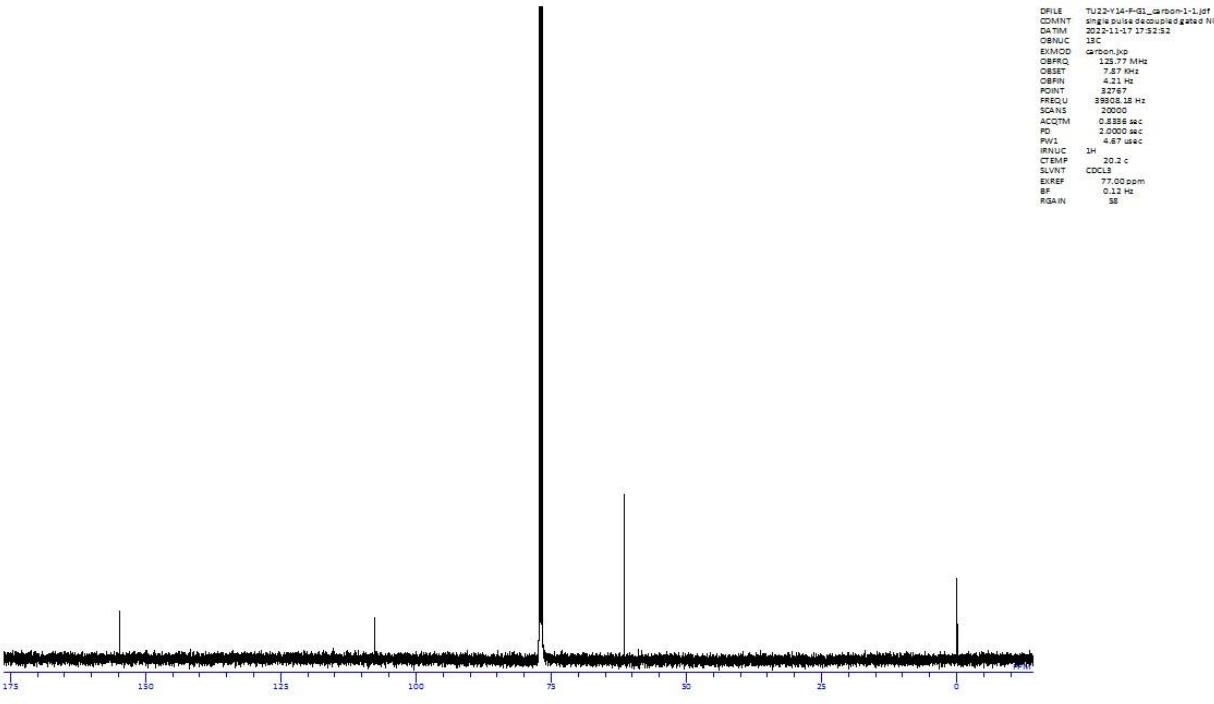

Fig. 34 ^{13}C NMR spectrum of BSeD(OMe)-Br in $CDCl_3$ at room temperature.

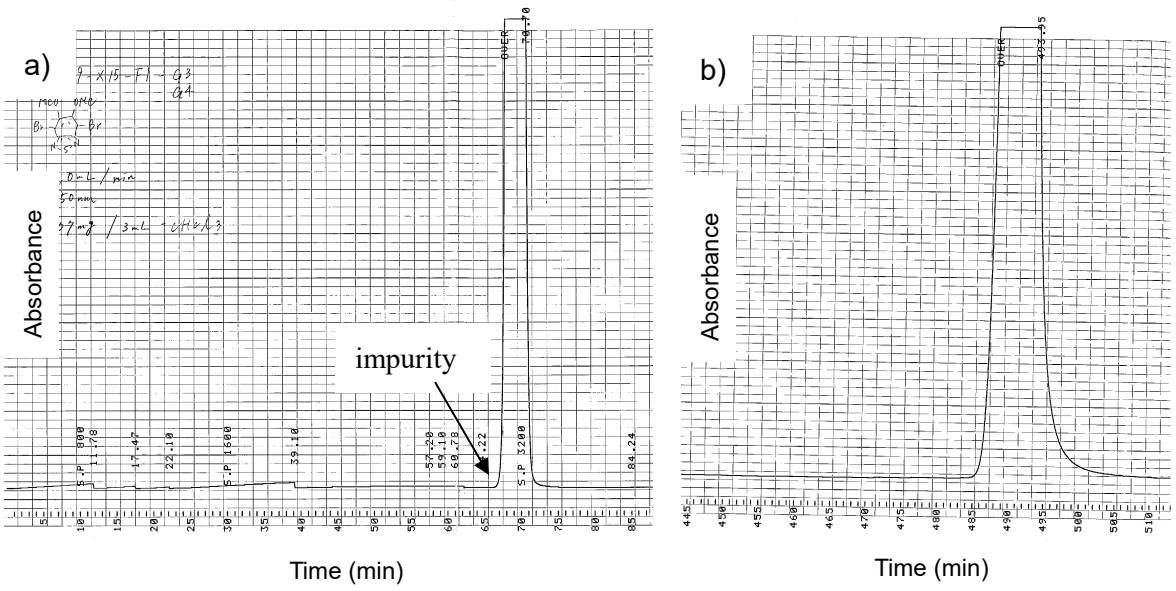

Fig. 35 GPC trace of BTD(OMe)-Br: (a) first cycle and (b) seventh cycle (after removing the impurity). The vertical axis is the absorbance at 350 nm: due the large amount of sample the vertical axis exceeded value 2 of the absorbance.

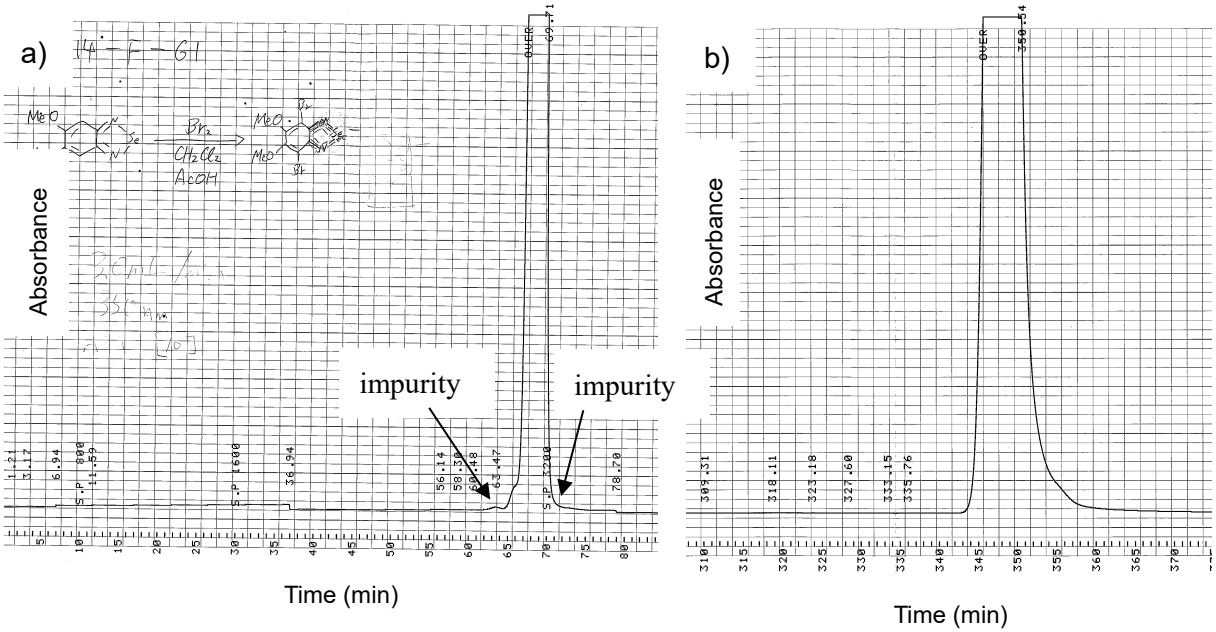

Fig. 36 GPC trace of BSeD(OMe)-Br: (a) first cycle and (b) sixth cycle (after removing the impurity). The vertical axis is the absorbance at 350 nm: due the large amount of sample the vertical axis exceeded value 2 of the absorbance.